Collisional and radiative properties of the H_2 $E,F\,^1\Sigma_g^+$ state

Daniel J. Kligler* and Jeffrey Bokor†
Department of Electrical Engineering, Stanford University, Stanford, California 94305

Charles K. Rhodes
Department of Physics, University of Illinois at Chicago Circle, Chicago, Illinois 60680

(Received 31 July 1979)

Collisional and photoabsorption properties of electronically excited molecular hydrogen are studied by means of selective excitation of the H_2 ($E,F\,^1\Sigma_g^+$) double minimum state. The $v=2$ level of the inner well of the E,F state is populated by two-photon absorption of ArF* laser radiation at 193 nm. Intracavity prisms are used to narrow the laser linewidth and tune the laser to excite single rotational levels selectively. Both H_2 and HD have been excited in this manner, but the D_2 absorption lines are outside the laser tuning range. The population densities of the E,F rovibrational levels are measured by monitoring the near-infrared $E,F\,^1\Sigma_g^+ \rightarrow B\,^1\Sigma_u^+$ fluorescent emission. The E,F-state radiative lifetime, electronic and rotational collisional relaxation rates, and photoionization cross section at 193 nm are measured. The large electronic quenching cross section (~ 100 Å^2) observed is compared to a Born approximation calculation of inelastic scattering in the H_2 ($E,F\,^1\Sigma_g^+$) system and is found to be due to collisional population of the $C\,^1\Pi_u$ state. Observations of vacuum-ultraviolet $C\,^1\Pi_u \rightarrow X\,^1\Sigma_g^+$ emission support this conclusion. The rotational relaxation cross sections are $\lesssim 0.2$ Å for H_2, but are much larger in HD (~ 10 Å^2).

I. INTRODUCTION

In an earlier Letter,[1] the first selective population of a gerade excited state of H_2, the $E,F\,^1\Sigma_g^+$ state, was reported. In that work it was demonstrated that multiphoton absorption of ArF* laser radiation at 193 nm could be used to create substantial populations in states whose excitation energies were far in the vacuum ultraviolet (vuv)—corresponding to single-photon wavelengths below 100 nm. Two-quantum absorption in the reaction

$$H_2(X\,^1\Sigma_g^+) + 2\gamma(193\text{ nm}) \rightarrow H_2(E,F\,^1\Sigma_g^+) \quad (1)$$

was used to excite the E,F state and its near infrared (ir) fluorescent emission

$$H_2(E,F\,^1\Sigma_u^+) \rightarrow H_2(B\,^1\Sigma_u^+) + \gamma(\sim 800\text{ nm}) \quad (2)$$

was monitored to make the first measurements of collisional and radiative properties of that state.

Kinetic studies of the hydrogen molecule are of particular interest and importance because of hydrogen's central position in the theory of molecular physics and quantum chemistry. Molecular hydrogen has been studied extensively from a theoretical point of view, but few experimental data on the collisional properties of the excited states exist because of the difficulty of selective excitation. Therefore, we have here extended and refined the studies of the E, F state discussed in Ref. 1, as well as made further comparisons of our results with theoretical predictions.

This report will present both experimental and new theoretical results concerning the relaxation and photoabsorption properties of the $E,F\,^1\Sigma_g^+$ state. Section II will first discuss the manifold of states excited in these experiments. Section III will outline the experimental apparatus and procedures. Measurements of radiative and collisional electronic relaxation rates of the $E,F\,^1\Sigma_g^+$ state will be reviewed in Sec. IV, and the mechanism of electronic quenching will be discussed and compared to a Born-approximation calculation of the electronic-quenching cross section derived here. Section V describes experimental determination of the cross section for three-photon ionization of H_2, which again is compared with theory. Finally, results obtained using rotationally resolved excitation and fluorescence detection to measure rotational relaxation rates in H_2 and HD are presented in Sec. VI.

II. EXCITATION MANIFOLD

As shown in Fig. 1, $E,F\,^1\Sigma_g^+$ is the first excited gerade singlet state of the hydrogen molecule.[2] This state was originally thought to be two separate states,[3] until Davidson pointed out its double-minimum character.[4] Kolos and Wolniewicz,[5] Wolniewicz and Dressler,[6] and Alemar-Rivera and Ford[7] have performed accurate calculations of the E,F potential curves and vibronic states.

The double minimum of the E,F state arises from the avoided crossing of the $1s\sigma 2s\sigma$ and the $F(2p\sigma)^2$ curves.[5] Thus, in terms of molecular orbitals, the E,F electronic wave function is almost exclusively $1s\sigma 2s\sigma$ in the inner well, while in the outer well it is mostly $(2p\sigma)^2$. At larger internuclear separation, the state has ionic character in the separated-atom representation (correlates to $H^+ + H^-$). However, due to an avoided crossing at

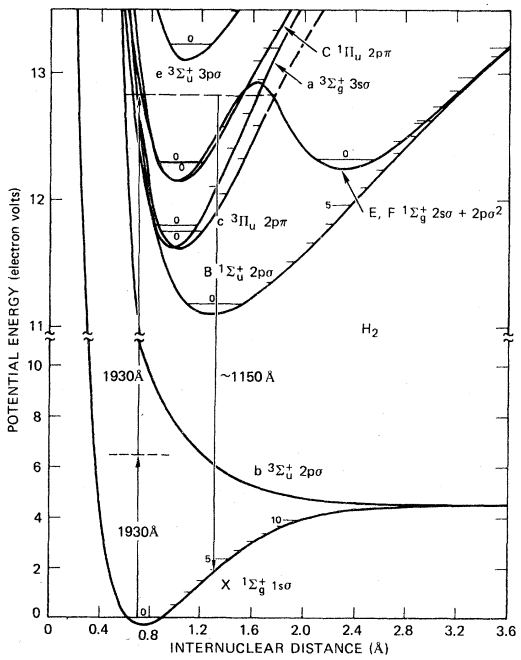

FIG. 1. Energy-level diagram of H_2 showing the X, B, C, and E, F states of interest in this experiment, as well as other states in this energy range, based on potential curves in T. E. Sharp, At. Data 2, 119 (1971). Note the change in vertical scale above 10 eV.

large separation, the E,F state dissociates to $H(1s)+H(2s)$.

Two other states are important in these studies, $B^1\Sigma_u^+$ and $C\,^1\Pi_u$. The $B\,^1\Sigma_u^+$ state serves both as the dominant intermediate state in two-photon absorption to $E,F\,^1\Sigma_g^+$ and as the final state for near-ir emission originating from $E,F\,^1\Sigma_g^+$. At small internuclear separation, $B\,^1\Sigma_u^+$ has $1s\sigma 2p\sigma$ character,[8] while at larger separations the state is mainly ionic and nearly degenerate with E,F. It dissociates to $H(1s)+H(2p)$. The $C\,^1\Pi_u$ state[9] is almost purely the $1s\sigma 2p\pi$ Rydberg level. In analogy to the degeneracy of the $2s$ and $2p$ atomic levels, $C\,^1\Pi_u$ $(2p\pi)$ and the $E\,^1\Sigma_g^+$ $(2s\sigma)$ inner well of the E,F state are nearly degenerate. The $B\,^1\Sigma_u^+$ and $C\,^1\Pi_u$ states may relax radiatively to the $X\,^1\Sigma_g^+$ ground state in the well-known vuv Lyman and Werner bands, respectively. Howeever, $E,F \rightarrow X$ radiation is strictly forbidden by the $g \longleftrightarrow u$ selection rule (except in the isotopically mixed species, such as HD)[10]; thus, the E,F state may radiate only in the near ir to $B\,^1\Sigma_u^+$ and is consequently quasimetastable.

As we shall discuss later, the ArF* laser used in these experiments had an untuned linewidth of ~170 cm^{-1} centered at 193.4 nm and, by means of an intracavity prism system, could be tuned from 192.6 to 194.2 nm. It is thus expected that transitions in the energy range ~103 000 to 103 800 cm^{-1} may be excited by two-photon absorption. For the $X\,^1\Sigma_g^+ \rightarrow E,F\,^1\Sigma_g^+$ transition in hydrogen, with the $B\,^1\Sigma_u^+$ dominant intermediate state, and using linearly polarized light, Q-branch rotational transitions are generally strongest, though O- and S-branch transitions are also allowed.[11] Table I lists the energy ranges for the O-, Q-, and S-branch transitions from the lowest three rotational levels (which are populated at 300°K) of the ground vibrational state of H_2 to the $E,F\,(v=2)$ level. From the energies listed, we expect strong two-photon excitation of several E,F $(v=2)$ rotational levels in H_2, weaker excitation in HD, where the transitions are to the red of the laser line center, and no excitation in D_2, whose levels are outside the laser's tuning range. Note that all other states

TABLE I. H_2 transition frequencies.

		H_2 [a]	HD [b]	D_2 [c]
Two-photon transition energy range (cm^{-1}) for $X\,^1\Sigma_g^+$ $(v=0) \rightarrow$ $E,F\,^1\Sigma_g^+$ $(v=2)$, $J'=0-3$	Q branch	103 282–103 552	102 926–103 221	102 555–102 741
	S branch	103 674–103 869	103 239–103 370	102 817–102 855
	O branch	102 893–103 198	102 729–102 954	102 410–102 561
Wavelengths of $E,F \rightarrow B$ emission bands (nm)				
(2, 1)		830	850	890
(2, 0)		750	780	830

[a] Reference 34.
[b] Reference 10.
[c] G. H. Dieke and S. P. Cunningham, J. Mol. Spectrosc. 18, 288 (1965).

in the vicinity of ~12.8 eV are forbidden for two-quantum excitation from the ground $X\,^1\Sigma_g^+$ state by either parity, spin, or both, and Franck-Condon factors for absorption to the outer minimum are unfavorable. These points are clearly evident in Fig. 1.

III. EXPERIMENT

The experimental apparatus used in this work has largely been described elsewhere.[12,13] The focused beam of a transverse-discharge-pumped argon fluoride laser (Lambda Physik EMG-500) was used to excite hydrogen samples in the experimental cell. The sample fluorescence following irradiation was collected at right angles to the laser beam. When time-resolved detection was desired, the fluorescent emission was focused onto the photocathode of a RCA C31034A photomultiplier tube[12]; the output of the tube was recorded by a transient digitizer (Tektronix R7912), which was interfaced to a PDP 11/34 computer. In this case, wavelength discrimination was provided by 10-nm-bandpass interference filters. Better wavelength resolution (~2 Å) in detection was achieved, at the expense of temporal information, by using an optical multi-channel analyzer (OMA) to observe the fluorescence spectrum.[13] This apparatus, which was also interfaced to the computer, generated a plot of time-integrated emission intensity versus wavelength, but with lower overall detection efficiency than the photomultiplier system.

The untuned ArF* laser emitted 100 mJ pulses of ~10 nsec [full width at half-maximum(FWHM)] duration in a band about 7 Å wide. Because of the high gain of the laser medium, the beam was oblong (about 2×0.7 cm^2) and had divergence ~5 mrad. In order to excite single rotational levels of hydrogen selectively, a laser line-narrowing and tuning system of the type first described by Loree *et al.*,[14] consisting of two intracavity fused silica prisms, was constructed. A slit of adjustable width was placed at the opposite end of the laser cavity from the prisms in order to create a well-defined optical axis. With these modifications, the laser linewidth was reduced to ~1Å (25 cm^{-1}), with a tuning range ~16 Å, roughly the range of the ArF* spontaneous emission. Laser energy near the line center (193.4 nm) was between 30% and 50% of the untuned energy, but dropped off to a few percent far in the wings. The laser wavelength was measured by a second OMA, which was calibrated with 0.5 Å accuracy by means of the dips in the laser emission spectrum due to O_2 absorption lines in the (4, 0) vibrational band of the Schumann-Runge system ($B\,^3\Sigma_u^- \rightarrow X\,^3\Sigma_g^-$).[14-16]

Using this apparatus, samples of H_2, HD, and D_2 were irradiated at pressures ranging from 10 mtorr to several atm. As predicted by the spectroscopic data in Table I, upon irradiation by the untuned laser, strong near-ir emissions were observed in H_2, weaker emissions in HD, and none in D_2. When the laser was tuned into closer resonance with the HD $E,F\,^1\Sigma_g^+ \rightarrow X\,^1\Sigma_g^+$ (2, 0) absorption band, ir emissions nearly as strong as those in H_2 were observed. At low laser intensity ($\lesssim 10^8$ W/cm^2), the intensity of the fluorescent signals was determined to vary as the square of the incident laser intensity, the characteristic signature of a two-photon absorption.

The near-infrared emission observed in this manner is attributed to radiative decay from the initially excited $v=2$ level of the $E,F\,^1\Sigma_g^+$ state (inner minimum) at ~ 12.8 eV to the $B\,^1\Sigma_u^+$ ($v=0$ and $v=1$) vibrational levels in reaction (2). The approximate wavelengths of the (2, 0) and (2, 1) emission bands are listed in Table I. The ratio of observed emission intensity in the H_2 (2, 1) band to that in the (2, 0) band was found to be 1.4 ± 0.2, which agrees well with theoretical calculations of the Einstein A coefficients[17] giving $A_{2,1}/A_{2,0} = 1.51$. A rotationally resolved $E,F \rightarrow B(2,0)$ spectrum, observed following excitation of H_2 by the untuned laser is shown in Fig. 2. Emission originating from $J'=0, 1$, and 2 is observed, but $J'=3$ is not excited. More than 90% of the emission is in the $P(2)$ and $R(0)$ lines, indicating that $J'=1$ is predominantly populated by the untuned laser. The reasons for this behavior, as well as results of excitation using a line-narrowed source, will be discussed in Sec. VI of this paper.

Finally, we should make mention of the vibrational bands that we did not observe in these ex-

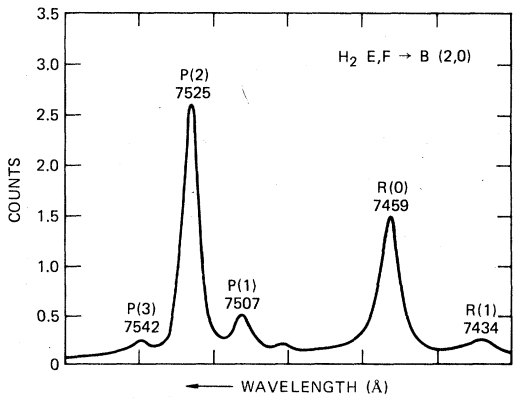

FIG. 2. H_2 $E,F \rightarrow B(2, 0)$ fluorescence spectrum detected by the OMA following ArF* laser broadband excitation. Five rotational lines are observed. Resolution is 4 Å; H_2 pressure 2 atm.

periments. Any emissions emanating from $v=0$ or $v=1$ of the inner well of $E,F\,^1\Sigma_g^+$, which might arise due to vibrational relaxation of $v=2$, as well as emissions from vibrational levels in the outer well, would be outside the spectral sensitivity of our photomultiplier and were not detected. However, Fink and co-workers[18] have measured vibrational relaxation rates for the B state in HD, and they are approximately two orders of magnitude smaller than the total quenching rate for H_2 $(E,F\,^1\Sigma_g^+;\ v=2)$ measured in Ref. 1. Assuming that vibrational relaxation is not markedly different in the E,F state in H_2, we expect that it does not play an important role in the collisional deactivation of H_2 $(E,F\,^1\Sigma_g^+;\ v=2)$. Similarly, our system was insensitive to emissions terminating on $v''\geq 2$. This is not of consequence, since the probabilities for these $(2,v'')$ transitions, calculated from the Franck-Condon factors of Spindler,[19] are negligible by comparison with the (2, 1) and (2, 0) transitions.

IV. MECHANISMS OF ELECTRONIC RELAXATION

In earlier work[1] the decay rate of the H_2 $E,F\rightarrow B$ fluorescence was measured as a function of pressure, and the radiative and collisional electronic relaxation rates of the E,F state were determined from these data. The E,F-state radiative lifetime was found to be 100 ± 20 nsec in excellent agreement with the calculated value[17,19] of 90 nsec. The total deactivation rate due to collisions with ground-state H_2 molecules was found to be $(2.1\pm 0.4)\times 10^{-9}$ cm^3/sec; with helium as the collision partner, the rate was $(0.8\pm 0.4)\times 10^{-9}$ cm^3/sec. On the basis of the large (nonreactive) helium quenching rate, it was hypothesized that the dominant electronic relaxation channel was

$$H_2(E,F\,^1\Sigma_g^+)+H_2(X\,^1\Sigma_g^+)\rightarrow H_2(C\,^1\Pi_u)+H_2(X\,^1\Sigma_g^+)\ , \tag{3}$$

followed by the rapid radiative decay (~1 nsec) of the $C\,^1\Pi_u$ state. In this section we shall calculate the cross section for reaction (3) for comparison with the measured H_2 quenching rate.

The $E,F\,^1\Sigma_g^+$ (inner minimum) $\rightarrow C\,^1\Pi_u$ transition in H_2 is remarkable in its resemblance to the hydrogen atomic $2s\rightarrow 2p$ fine-structure transition. The potential curves shown in Fig. 1 illustrate that these two molecular states are nearly degenerate in the E,F inner minimum. Thus, the $E,F\rightarrow C$ transition requires only a small perturbation in the nuclear motion. Calculations by Kolos and Wolniewicz[5,9] indicate that at the internuclear separations of interest here (~1 Å), the E $(2s\sigma)$ and C $(2p\pi)$ molecular orbitals maintain a strong resemblance to their atomic counterparts. Consequently, scattering in reaction (3) should resemble the atom-molecule interaction

$$H(2s)+H_2(X\,^1\Sigma_g^+)\rightarrow H(2p)+H_2(X\,^1\Sigma_g^+)\ . \tag{4}$$

This atomic quenching has been studied both experimentally[20,21] and theoretically.[22,23]

Since the $2s$ and $2p$ states of hydrogen are connected by a strong dipole moment $(\mu=3ea_0)$, while ground-state H_2 has a permanent quadrupole moment, a dipole-quadrupole potential is used for the transition Hamiltonian for reactions (3) and (4). Because of the long range of this interaction (R^{-4}) and the near degeneracy of initial and final channels, the problem may be treated by the first Born approximation. We shall now outline a Born-approximation calculation of the scattering matrix for the dipole-quadrupole interaction of H_2^* and H_2 and derive from this the inelastic-scattering cross section for process (3). A more complete derivation can be found in Ref. 24.

We begin by defining the T matrix for scattering from state α to state α' as

$$T_{\alpha'\alpha l'lm'0}=S_{\alpha'\alpha l'lm'0}-\delta_{\alpha'\alpha}\delta_{l'l}\delta_{m'0}\ , \tag{5}$$

where S is the standard scattering matrix relating the amplitude of scattered waves in channels $(\alpha',\ l',m')$ to that of the incident wave in channel $(\alpha,l,0)$. Here $l(l')$ and $m(m')$ give the initial (final) orbital angular momentum of the projectile relative to the target, but we set $m=0$ by taking the initial velocity parallel to the z axis. Taking the interaction potential V, we write

$$V_{\alpha'\alpha}=\langle\psi_{\alpha'}|\,V\,|\psi_\alpha\rangle\ , \tag{6}$$

where $\psi_\alpha(\psi_{\alpha'})$ is the initial (final) state of the system, including electronic, vibrational, and rotational components. Now we write the first Born-approximation expression for the T matrix[25]:

$$T_{\alpha'\alpha l'lm'0}=\frac{-4mi\,(kk')^{1/2}}{\hbar^2}\int j_{l'}(k'R')Y^*_{l'm'}(\theta',\phi')V_{\alpha'\alpha}(\vec{R})j_l(kR')Y_{l0}(\theta',\phi')R'^2\,dR'\,d\Omega'\ . \tag{7}$$

In this expression k (k') is the initial (final) projectile vector, and the j_l are the spherical Bessel functions.

The classical dipole-quadrupole expression[26] for the interaction of the excited electron's $2s\sigma\rightarrow 2p\pi$ transition dipole moment with the H_2 ground-state

quadrupole moment is

$$V_{dq}=\frac{4\pi Q r}{R^4}\sum_{\mu} C(123;\mu-\mu)Y_{1,\mu}(\theta_{e'}\phi_e)\times Y_{2,-\mu}(\theta_2,\phi_2)\ . \tag{8}$$

Here Q is the ground-state quadrupole moment, R is the intermolecular separation, r is the coordinate of the excited electron, C is a Clebsch-Gordan coefficient, and (θ_e,ϕ_e) and (θ_2,ϕ_2) give the angular orientations of the excited electron position and the ground-state molecule's internuclear axis, respectively, referred to the (time-varying) intermolecular axis. V_{dq}, proportional to R^{-4}, is the longest-range possible potential in our system; dipole-induced dipole and Van der Waals potentials both vary as R^{-6}.

We now write the wave function for the two-molecule system (neglecting the electronic and vibrational states of the ground-state H_2):

$$\psi=|\psi_e\rangle|\psi_v\rangle|j_1M_1\rangle|j_2M_2\rangle|lm\rangle\ . \tag{9}$$

We shall continue to indicate initial state by unprimed and final state by primed symbols. $|\psi_e\rangle=|2s\sigma\rangle$; $|\psi_e'\rangle=|2p\pi\rangle$; and $|\psi_v\rangle$, $|\psi_v'\rangle$ are the vibrational states. j_i and M_i indicate the molecules' internal rotational states, where subscript 1(2) indicates the excited (ground-state) molecule.

Inserting expressions (8) and (9) into Eq. (7) and transforming the angular coordinates from the time-varying collision frame to space-fixed and molecule-fixed axes yields an expression for the T matrix:

$$T_{\alpha'\alpha l'lm'0}=-\frac{4mi}{\hbar^2}\frac{(4\pi)^{3/2}}{\sqrt{7}}Q\mu\langle\psi_{v'}|\psi_v\rangle\langle l'|R^{-4}|l\rangle\sum_m\sum_{m_1',m_2'}(-1)^{m_1'+m_2'}C(123;m_1'm_2')\langle 1M|1m|00\rangle$$
$$\times\delta_{M,\pm1}\langle j_1'M_1'|D^{(1)}_{m,m_1'}|j_1M_1\rangle\langle j_2'M_2'|2m_2'|j_2M_2\rangle\langle l'm'|3m_1'+m_2'|l0\rangle\ . \tag{10}$$

Here $\mu\simeq 3ea_0$ is the $2s\to 2p$ dipole moment, and $\langle\psi_v'|\psi_v\rangle$ is the Franck-Condon factor $q_{v',v}$. $D^{(1)}_{m,m'}$ is a rotation-matrix element.[27] The radial integral is

$$\langle l'|R^{-s}|l\rangle\equiv(kk')^{1/2}\int_0^\infty j_{l'}(k'R)R^{-s}j_l(kR)R^2\,dR\ , \tag{11}$$

which contains the resonance dependence of the scattering. The $\delta_{M,\pm1}$ in Eq. (10) arises from the fact that the $M=0$ term would connect $|2s\sigma\rangle$ to $|2p\sigma\rangle$, which is the $B\,^1\Sigma_u^+$ state, not included in this calculation. We note that scattering to $B\,^1\Sigma_u^+$ is allowed, but unimportant compared to reaction (3) due primarily to the substantially smaller Franck-Condon factors[19] for $E\to B$ transitions of small energy defect.

If we define the impact parameter as $b=(2l+1)/2k$, then we may obtain the scattering probability for a given b by summing $|T_{\alpha'\alpha l'lm'0}|^2$ over final angular momentum states and averaging over initial rotational projections (M_1 and M_2).[25] The result obtained is a simplified sum over l', independent of initial rotational states j_1 and j_2:

$$P(b)=\left(\frac{m\mu Q_{v'v}}{\hbar^2}\right)^2\frac{32}{3}\sum_{l'}C(l3l';00)^2\times\langle l'|R^{-4}|l\rangle^2\ . \tag{12}$$

This expression is identical to the probability for atomic $2s\to 2p$ scattering[25] except for the Franck-Condon factor $q_{v'v}$ and an additional factor of $\frac{2}{3}$ here. This latter factor arises from our consideration of transitions only to the two $2p\pi$ states, while in the atomic case transitions to all three $2p$ levels ($M=\pm1$ and 0) are included.

The cross section for the inelastic-scattering process is now found by integrating

$$\sigma(k)=\int_0^\infty 2\pi P(b)b\,db\ . \tag{13}$$

However, $P(b)>1$ for small b, because the Born approximation breaks down at close range. Hence, as suggested by Cross and Gordon[25] and by Slocomb *et al.*,[23] we set $P(b)=1$ for $b<b_h$, where b_h is given by $P(b_h)=1$ from Eq. (12). Now

$$\sigma=\pi b_h^2+2\pi\int_{b_h}^\infty P(b)\,b\,db\ . \tag{14}$$

A simple computer program was written to calculate scattering probability from Eq. (12) and cross section from Eq. (14) as functions of initial projectile momentum and detuning of initial and final states. The radial integral of Eq. (12) was solved explicitly in terms of the hypergeometric function.[25,28] The energy detuning was obtained from spectroscopic data on the energies of the rotational levels in the $E,F\,^1\Sigma_g^+$ ($v=2$) and $C\,^1\Pi_u$ ($v=2$) manifolds. These data, shown graphically in Fig. 3, indicate that the $J=1$ levels, from which >90% of the observed emission originates (see Fig. 2 and ensuing discussion), are separated in energy by only 22 cm^{-1}. The other data that must go into calculation are the H_2 ground-state quadrupole moment,[29] $Q=0.484$ a.u., the Franck-

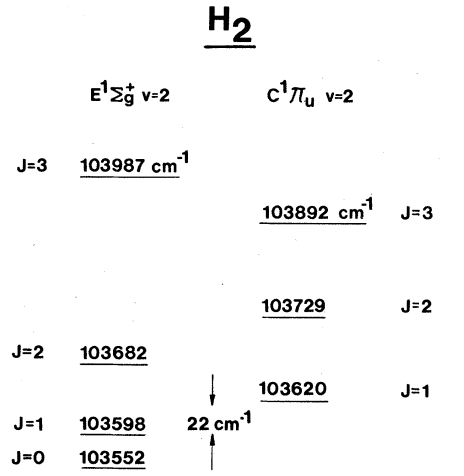

FIG. 3. Energies of rotational levels in H_2 $E, F\,^1\Sigma_g^+$ (inner minimum, $v=2$) and $C^1\Pi_u$ ($v=2$) (Ref. 34).

Condon factor,[30] $q_{2,2}=0.794$, and the projectile velocity. Averaging the product of velocity and cross section over a Boltzmann distribution of kinetic energies gives a rate constant for process (3) of 2.3×10^{-9} cm^3/sec at 300 °K. This result agrees remarkably well with the experimental determination of $(2.1\pm0.4)\times10^{-9}$ cm^3/sec, and supports our hypothesis that reaction (3) is the primary mechanism in collisional deactivation of H_2 ($E, F\,^1\Sigma_g^+$; $v=2$).

These theoretical conclusions are lent further support by experimental observation of $C\,^1\Pi_u \rightarrow X\,^1\Sigma_g^+$ vuv Werner-band emissions following two-photon excitation of the E, F state. Figure 4

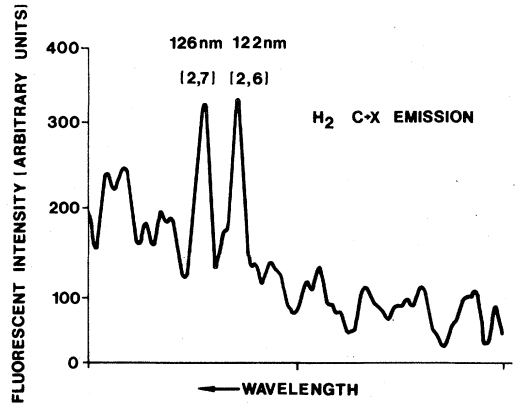

FIG. 4. H_2 $C\,^1\Pi_u \rightarrow X\,^1\Sigma_g^+$ vuv Werner-band fluorescence spectrum detected by OMA following ArF* laser excitation of the E, F state. The (2,6) and (2,7) vibrational bands are observed, but the (2,5) band is beyond the wavelength cutoff of the detection system. The rotational structure is not resolved.

is a spectrum of this emission near 125 nm, showing the (2,6) and (2,7) vibrational bands of the $C \rightarrow X$ fluorescence. [The (2,5) band, which should be present, is beyond the transmission cutoff of our optical system.] These observations of emission in the Werner bands confirm that large populations are created in the $v=2$ level of the $C\,^1\Pi_u$ state following $E, F\,^1\Sigma_g^+(v=2)$ two-photon excitation. The absence of emission from other C-state vibrational levels confirms our model of electronic quenching, as well as the contention that vibrational relaxation is much slower than the electronic.

Because of the near degeneracy of the E and C states, at pressures above ~ 20 torr these levels will reach thermal equilibrium within ~1 nsec of excitation. (The principle of detailed balance requires that the $C \rightarrow E$ quenching rate be nearly equal to the $E \rightarrow C$ rate.) Under these circumstances, when other losses are neglected, the probability that a H_2 molecule in the $E, F\,^1\Sigma_g^+$ state will radiate in its $E, F \rightarrow B$ ir bands is simply τ_C/τ_E, where τ_E and τ_C are the radiative lifetimes of the E and C states, respectively. From the theoretical calculations of Allison and Dalgarno for the $C\,^1\Pi_u \rightarrow X\,^1\Sigma_g^+$ transition probabilities,[31] we obtain $\tau_C(v=2)=0.88$ nsec. The effective radiative lifetime of a molecule excited to the E, F state at high pressure is given by a rate equation analysis:

$$\tau_{\text{eff}} = \frac{2\tau_E\tau_C}{\tau_E+\tau_C} \,. \tag{15}$$

In our case, for $\tau_E \gg \tau_C$, $\tau_{\text{eff}} \cong 2\tau_C$. This analysis will be important in our later estimates of rotational relaxation and photoionization rates.

V. PHOTOIONIZATION OF THE E,F STATE

While the electronic relaxation processes we have examined are quite rapid, at higher laser intensities the fastest loss process—and hence the limiting factor in achievable excitation density—is photoionization of the excited molecules. This is a pervasive problem in two-photon studies using rare gas halide lasers, because three ArF* photons (= 19.2 eV) are sufficient to ionize almost all atoms and molecules. While the characteristic signature of a two-photon process is a signal which grows as the square of laser intensity, when photoionization is prevalent, the signal "saturates" and grows only linearly with intensity; meanwhile, the laser energy is increasingly channeled into ion production.

The nature of this behavior may be seen in a rate equation analysis of the two-photon excited state density N^*:

$$\frac{dN^*}{dt} = \frac{\alpha I^2}{\hbar\omega}[H_2] - \frac{N^*}{\tau_{\text{eff}}} - \frac{\sigma_{\text{pi}} I}{\hbar\omega} N^* \,. \tag{16}$$

Here $\alpha = \sigma/I$ (cm^4/W) is the two-photon absorption coefficient,[12] I is the laser intensity (W/cm^2), ω is the laser frequency, and σ_{pi} is the photoionization cross section for the excited state. At high pressure and high laser intensity, radiative and ionization losses are fast enough so that we can assume a steady-state solution to Eq. (16):

$$N^* = \frac{\alpha I^2 [H_2]}{\hbar\omega/\tau_{eff} + \sigma_{pi} I} \quad . \tag{17}$$

As noted earlier, $\tau_{eff} \simeq 2\tau_C = 1.8$ nsec at high pressure. This solution clearly shows the saturation of N^* at large I. (As a further note, while photoionization is a broadband process, two-photon absorption terminates on a discrete state. Hence, decreasing the laser linewidth, much broader in our case than the transition Doppler width, will increase α but not σ_{pi} and, thus, will increase the excitation efficiency and excited-state density.[13,32])

If we can measure the saturation of the two-photon signal with laser intensity, we can extract from these data the photoionization cross section for the excited state. We begin by using the fact that the ir fluorescent signal is simply $S = N^*/2\tau_E$ to rearrange Eq. (17):

$$\frac{I}{S} \propto \frac{\hbar\omega}{2\tau_c \alpha [H_2]} \frac{1}{I} + \frac{\sigma_{pi}}{\alpha [H_2]} = mI^{-1} + B \quad . \tag{18}$$

The significance of this equation is that if we now plot the quotient I/S from our data as a function of I^{-1}, we can extract the photoionization cross section σ_{pi}, from the ratio of intercept to slope, B/m, in our plot:

$$\sigma_{pi} = \frac{\hbar\omega}{2\tau_c} \frac{B}{m} \quad . \tag{19}$$

Figure 5 shows a measurement of the ir fluorescent signal as a function of laser energy, plotted in accordance with Eq. (18). The plot is fairly linear, and the nonzero intercept indicates that photoionization losses lead to the expected saturation of the signal at high laser intensity. On the basis of these data, we estimate that 8×10^{-19} $cm^2 \leq \sigma_{pi} \leq 4\times10^{-18}$ cm^2. This large uncertainty arises primarily from the uncertainty in converting the measured laser energy to the actual laser intensity at the focus. This estimate is, however, in agreement with the theoretical calculations of Cohn.[33] For photoionization from H_2 ($E,F\,^1\Sigma_g^+$; $v=2$) to H_2^+ ($X\,^2\Sigma_g^+$; $v=2$) at 6.4 eV (3.3) eV above threshold), Cohn calculates $\sigma_{pi} = 2.6\times10^{-18}$ cm^2. It must be noted, however, that this experiment does not actually measure the E,F-state photoionization cross section, but rather the cross section for photoionization of the collisionally mixed, E,F and C states.

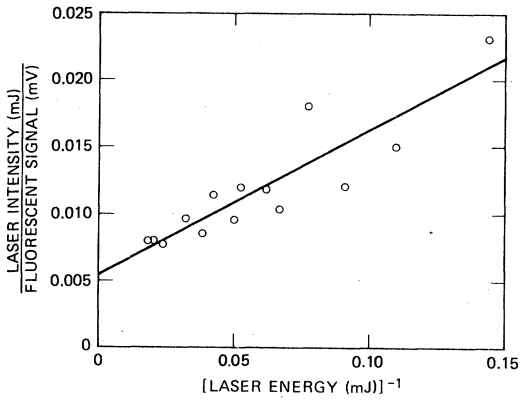

FIG. 5. Ratio of laser energy (193 nm) to fluorescent signal ($E,F \rightarrow B$, 830 nm), plotted as a function of the reciprocal of laser energy. Ratio of intercept to slope of the straight-line fit to the data is 0.05 mJ^{-1}.

VI. ROTATIONALLY SELECTIVE MEASUREMENTS

While we have observed very rapid electronic deexcitation processes in the H_2 E,F state, rotational relaxation is considerably slower. If the data of Fig. 2 are compared to a theoretical formula for the intensities of rotational lines in a vibrational band in thermal equilibrium,[11] it is found that even at the high pressure [20 psi (gauge)] at which this spectrum was taken, the rotational levels are not equilibrated.[13] On the contrary, Table II, which lists the ground-state equilibrium rotational populations and two-photon $X \rightarrow E,F$ transition energies for $J = 0$–3 (populated at 300°K), demonstrates that the relative intensities of the $E,F \rightarrow B$ rotational lines are due to a nearly total absence of rotation-changing collisions in the excited state. Thus, since only the $Q(0)$ and $Q(1)$ excitation transitions fall squarely within the two-photon laser band, only $J = 0$ and $J = 1$ levels are seen to emit substantially in the spectrum of Fig. 2.

TABLE II. Rotational level populations (relative to $J = 0$) and frequencies (cm^{-1}) of $H_2 X\,^1\Sigma_g^+$ ($v = 0$) $\rightarrow E,F\,^1\Sigma_g^+$ ($v = 2$, inner well) two-photon transitions.

		Branch		
J	$n(J)/n(0)$	O	Q	S
0	1		103 552	103 682
1	4.9		103 479	103 869
2	0.83	103 197	103 328	103 797
3	0.52	102 892	103 282	103 673

In order to measure the rate of this very slow rotational relaxation, we installed the prism system and tuned the laser to excite selectively each of the first four rotational levels of $H_2(E, F\,^1\Sigma_g^+; v=2)$ in turn. We then attempted to observe emission from J levels other than the one excited. The results of these observations are shown in Fig. 6. In no case was any rotational relaxation evident above the ~10% noise level in the measurements.

We can use this signal-to-noise ratio to set an upper bound on $2 \rightarrow 0$ and $3 \rightarrow 1$ rotational relaxation rates. (We do not expect any odd $\rightarrow$ even relaxation because of the strict ortho/para separation in homonuclear diatomics.[11]) Assuming that the laser is tuned to excite the $J+2$ level and that the J th level is populated only by rotational relaxation from $J+2$, which is much slower than electronic relaxation, the ratio of populations in the two levels is given by a steady-state analysis:

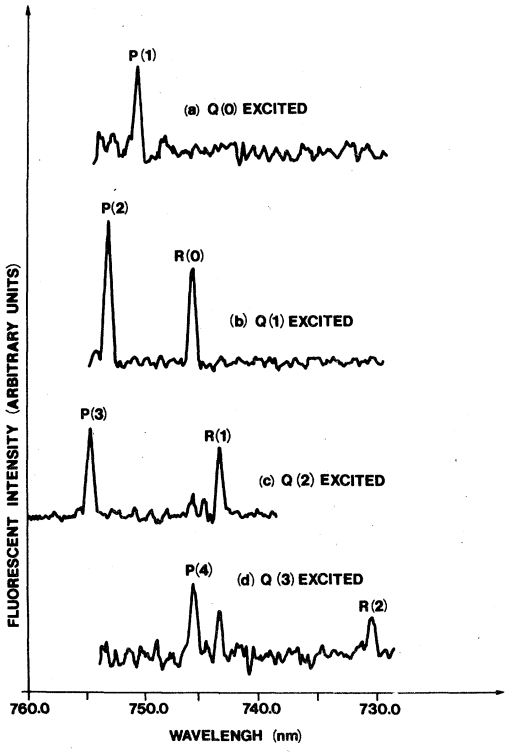

FIG. 6. H_2 $E, F \rightarrow B$ (2, 0) fluorescence spectra detected by OMA following rotationally selective excitation by a line-narrowed ArF* laser. H_2 pressure is 20 psi (gauge). Excitation line: (a) $Q(0)$, (b) $Q(1)$, (c) $Q(2)$, (d) $Q(3)$. Appearance of $R(1)$ emission in (d) arises from direct excitation of the $Q(2)$ absorption line, due to the presence of some laser oscillation at this frequency when laser is tuned to $Q(3)$, not from rotational relaxation.

$$\frac{n_J}{n_{J+2}} \simeq \frac{k^{J+2,J}[H_2]}{R_L} . \tag{20}$$

In this equation, $R_L = \sigma_{pi} I/h\omega + 1/(2\tau_C) \simeq 3$ nsec^{-1} is the electronic loss rate, and $k^{J+2,J}$ is the two-body rate coefficient for rotational transitions from level $J+2$ to level J. The ratio of rotational-level populations is also related to the fluorescent emission intensities S of the P lines originating in the J and $J+2$ rotational levels by[11]

$$\frac{S[P(J+1)]}{S[P(J+3)]} = \left(\frac{\nu_J}{\nu_{J+2}}\right)^4 \left(\frac{J+1}{J+3}\right)\left(\frac{2J+5}{2J+1}\right) \frac{n_J}{n_{J+2}} , \tag{21}$$

where ν_J and ν_{J+2} are the respective transition frequencies.[34] Finally, we observe in Fig. 6 that $S[P(2)]/S[P(4)]$ and $S[P(1)]/S[P(3)] \leq 0.1$, leading us to conclude on the basis of equations (20) and (21) that $k_R^{2,0} \leq 3\times10^{-12}$ cm^3/sec and $k_R^{3,1} \leq 6\times10^{-12}$ cm^3/sec. These rate constants are more than two orders of magnitude smaller than the observed electronic quenching rates for the E, F state.

Rotational relaxation will be greatly enhanced in the isotopically mixed species of hydrogen as shown by Heukels and Van de Ree.[35] First, the shift of the center of mass away from the center of charge has the net effect of slightly increasing the cross section for a given rotational transition. More importantly, however, additional channels open up in the mixed species that are forbidden in the homonuclear species. Specifically, $\Delta J = 1$ transitions are allowed in the heteronuclear case, while J must retain its parity in the homonuclear molecule, due to nuclear-spin-symmetry considerations. $\Delta J = 1$ transition cross sections are calculated[35] to be roughly one order of magnitude larger than the $\Delta J = 2$ cross sections for He-HT collisions in the ground electronic state, and the $\Delta J = 2$ transition cross section for He-D_2 collisions is calculated[35] to be roughly 40% smaller than for He-HT collisions.

Figure 7 shows the lower rotational levels of the HD $E, F\,^1\Sigma_g^+$ ($v=2$, inner well) and $C\,^1\Pi_u$ ($v=2$) states, with + and − signs to indicate the parities of the levels.[12] The rapid electronic collisions (studied in Sec. IV of this paper) that equilibrate the E, F and C levels of opposite symmetries are shown by bold arrows. The parity-changing rotational collisions, forbidden in H_2 and D_2, are indicated by the fine arrows. We shall now describe a measurement of the collisional rate of this latter process in HD.

In this experiment, the laser was tuned to the $Q(0)$ and $Q(1)$ two-photon excitation lines in HD, at 103 221 and 103 173 cm^{-1}, respectively.[10] Because the lines are closely spaced and located in the wing of the laser gain band, it was not possible

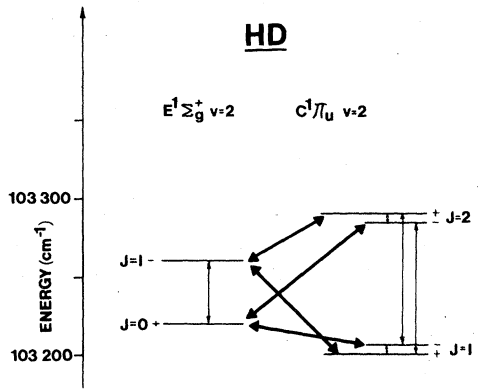

FIG. 7. Energies of lower rotational levels in HD ($E,F\,^1\Sigma_g^+$; inner well, $v=2$) and $C\,^1\Pi_u$; $v=2$. Bold arrows indicate rapid electronic quenching collisions, while fine arrows show slower rotational quenching paths. Lambda doubling in the C state [see Paul S. Julienne, J. Mol. Spectrosc. 48, 503 (1973)] is exaggerated for clarity.

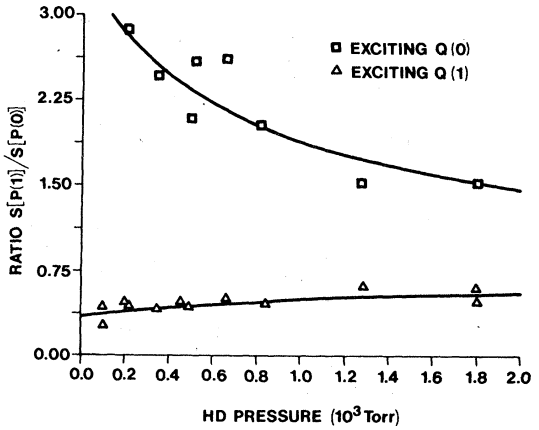

FIG. 8. Ratio of fluorescent intensity, S, of $P(1)$ line to that of $P(2)$ in the HD $E,F \rightarrow B(2,0)$ band following rotationally selective excitation by ArF* laser. For upper curve (boxes) the laser was tuned to excite primarily $J=0$, while for lower curve (triangles) laser was tuned to $J=1$.

to excite one line to the total exclusion of the other. Thus, the ratio of intensities in the $P(1)$ and $P(2)$ $E,F\,^1\Sigma_g^+ \rightarrow B\,^1\Sigma_u^+$ $(2,0)$ emission lines was measured as a function of HD pressure as the laser was tuned to excite predominantly $Q(0)$ or $Q(1)$ in turn. The results of these measurements are presented in Fig. 8, which, in contrast to Fig. 6, shows a clear tendency toward equilibrium at high pressure.

In order to extract rate constants $k_R^{0,1}$ and $k_R^{1,0}$ from these data, we examine a rate-equation model that includes both $1 \rightarrow 0$ and $0 \rightarrow 1$ rotational transitions:

$$\frac{dn_0}{dt} = R_p^{(0)}[\mathrm{HD}] - R_L^{(0)} n_0 - k_R^{0,1}[\mathrm{HD}] n_0 + k_R^{1,0}[\mathrm{HD}] n_1 \qquad (22)$$

$$\frac{dn_1}{dt} = R_p^{(1)} - R_L^{(1)} n_1 - k_R^{1,0}[\mathrm{HD}] n_1 + k_R^{0,1}[\mathrm{HD}] n_0 \qquad (23)$$

Here $R_p^{(0)}$ and $R_p^{(1)}$ are the two-quantum production rates of the $J=0$ and $J=1$ rotational levels, which will vary as the laser is tuned through the levels' excitation frequencies, and the $R_L^{(J)}$ are the corresponding electronic loss rates. We assume that the excited system is in quasi-steady state and that $R_L^{(1)} = R_L^{(0)} \simeq 3$ nsec^{-1}, as above, and solve for the ratio n_0/n_1:

$$\frac{n_0}{n_1} = \frac{k_R^{1,0}[\mathrm{HD}] + (R_p^{(0)}/R_p) R_L}{k_R^{0,1}[\mathrm{HD}] + (R_p^{(1)}/R_p) R_L} \ , \qquad (24)$$

where $R_p = R_p^{(0)} + R_p^{(1)}$. From a formula similar to Eq. (21), we have $S[P(1)]/[P(2)] = 1.5 n_0/n_1$. A three-parameter fit $[k_R^{1,0}$, $k_R^{0,1}/k_R^{1,0}$, and $R_p^{(0)}/R_p^{(1)}]$ of Eq. (24) to the data of Fig. 8 gives $k_R^{1,0} = (3 \pm 1) \times 10^{-10}$ cm^3/sec and $k_R^{0,1}/k_R^{1,0} = 2.1 \pm 0.5$. The fit is shown by the solid lines in the figure.

These rate constants do not refer simply to rotational transitions within the E,F manifold, but rather must be thought of as composite rates for all the transitions in Fig. 7 that are indicated by the fine arrows. However, the ratio $k_R^{0,1}/k_R^{1,0}$ is rigorously fixed theoretically by the principle of detailed balance[36] at 2.46, in good agreement with the experimental result.

For comparison with other experimental results, we transform the rate constants we have measured to average cross sections (by dividing by the mean thermal velocities at 300 K) and list these results in Table III. Our results in H_2^* are quite similar to the ground-state rotational-relaxation cross sections found by Jonkman *et al.*[37] The reasons that these cross sections are so small are that (i) these $\Delta J = 2$ transitions can proceed only through a quadrupole moment (in contrast to the strong-electric-dipole electronic transition that we studied) and (ii) the energy defects between initial and final states are comparable to or greater than thermal energies at the temperatures studied.

On the other hand, the cross section we measured in HD for $\Delta J = 1$ transitions is on the order of gas dynamic. Akins *et al.*,[38] also measured large collisional cross sections for rotational transitions in HD, although their results for the $B\,^1\Sigma_u^+$ state were still smaller than ours for the E,F state. The faster relaxation rate that we

TABLE III. H_2 and HD rotational relaxation cross sections.

	States	σ_R (Å^2)
This work	$H_2(E,F;v=2,J'=3,J''=1)$	≤ 0.12
	$(J'=2,J''=0)$	≤ 0.24
Jonkman *et al.* (Ref. 37)	$H_2(X;v=0,J'=2,J''0)$	0.10 (para-H_2, 170 K)
		0.26 (ortho-H_2, 77 K)
This work	$HD(E,F;v=2,J'=1,J''=0)$	14
Akins *et al.* (Ref. 38)	$HD(B;v=3,J'=2,J''=1)$	3.0

measured may be attributable to the contribution of coupling of the E,F levels through the C state manifold; no comparable coupling exists in the B or X states.

VII. CONCLUSIONS

In the experiments described here and in Ref. 1, we have, for the first time, selectively excited a gerade state of the hydrogen molecule, the quasimetastable $E,F\,^1\Sigma_g^+$ state in H_2 and HD. By line narrowing and tuning the ArF* laser excitation source, we have excited single rotational levels in H_2, and also achieved some rotational selectivity in HD. We have measured a number of the properties of the E,F state, including radiative lifetime, rates for collisional electronic quenching and rotational relaxation, two-photon-absorption cross section, and photoionization cross section. The radiative lifetime, electronic quenching rate for $H_2^*+H_2$ collisions, two-photon-excitation cross section, and excited-state photoionization cross section agree well with theoretical predictions. The rotational relaxation rates are roughly in line with other experimental results. These experiments demonstrate the utility of ultraviolet two-quantum absorption in investigating many different aspects of this most fundamental excited molecular system.

We have also studied in detail the mechanism of rapid electronic deactivation of H_2 $(E,F\,^1\Sigma_g^+)$ to the $C\,^1\Pi_u$ state. Our Born-approximation calculation of the cross section for this reaction gives very close agreement with the experimental determination of the quenching rate. Observations of vuv Werner-band emission further supports our model of the collisional processes involved here.

This experimental technique may be extended to further spectroscopic and collisional studies in excited H_2. Starting with two-photon-excited $E,F\,^1\Sigma_g^+$ molecules, a tunable dye laser can probe higher ungerade states, while from $C\,^1\Pi_u$ molecules created by collisional quenching of H_2 $(E,F\,^1\Sigma_g^+)$, higher gerade states may be reached as well. A two-photon-pumped laser operating on the H_2 Werner bands near 120 nm between $C\,^1\Pi_u$ $(v=2)$ and high vibrational levels of $X\,^1\Sigma_g^+$ is also feasible.[13] Finally, it may be possible to study such exotic processes as para-ortho conversion and production of HD* in four-center reactions of H_2^* and D_2 by this technique.

ACKNOWLEDGMENTS

We are grateful to D. L. Huestis for many useful discussions during the course of this work and to R. T. Hawkins for expert computer programming. The expert technical assistance of K. Skala and G. Murphy was invaluable in the contruction of the tunable ArF* laser. Daniel J. Kligler also wishes to thank the Molecular Physics Laboratory of SRI International for allowing him to use its PDP 11/40 computer for the calculations described in this paper and to acknowledge the helpful advice of W. H. Miller and A. P. Hickman in the scattering calculations. Jeffrey Bokor gratefully acknowledges the support of the Fannie and John K. Hertz Foundation. This work was supported by the National Science Foundation under Grant PHY-77-01849 and NSF78-27610, the Office of Naval Research under Grant N00014-78-C-0625, and the U. S. Department of Energy under Agreement No. ED-78-S-08-1603.

*Present address: Racah Institute of Physics, The Hebrew University, Jerusalem, Israel.
†Present address: Dept. of Physics, Univ. of Illinois at Chicago Circle, Chicago, Ill. 60680.

[1]Daniel J. Kligler and Charles K. Rhodes, Phys. Rev. Lett. 40, 309 (1978).
[2]T. E. Sharp, At. Data 2, 119 (1971).
[3]G. H. Dieke, J. Mol. Spectrosc. 2, 494 (1958).
[4]E. R. Davidson, J. Chem. Phys. 33, 1577 (1960); 35, 1189 (1961); R. J. Boye, J. Mol. Spectrosc. 26, 36 (1968).
[5]W. Kolos and L. Wolniewicz, J. Chem. Phys. 50, 3228 (1969).
[6]L. Wolniewicz and K. Dressler, J. Mol. Spectrosc. 67, 416 (1977).
[7]Jose D. Alemar-Rivera and A. Lewis Ford, J. Mol.

Spectrosc. 67, 336 (1977).
[8]W. Kolos and L. Wolniewicz, J. Chem. Phys. 48, 3672 (1968).
[9]W. Kolos and L. Wolniewicz, J. Chem. Phys. 43, 2429 (1965).
[10]I. Dabrowski and G. Herzberg, Can. J. Phys. 54, 525 (1976).
[11]Gerhard Herzberg, *Spectra of Diatomic Molecules* (Van Nostrand, Reinhold, New York, 1950).
[12]D. Kligler, D. Pritchard, W. K. Bischel, and C. K. Rhodes, J. Appl. Phys. 49, 2219 (1978).
[13]W. K. Bischel, J. Bokor, D. J. Kligler, and C. K. Rhodes, IEEE J. Quantum Electron. QE-15, 380 (1979).
[14]T. R. Loree, K. B. Butterfield, and D. L. Barker, Appl. Phys. Lett. 32, 171 (1978).
[15]R. Burnham and N. Djeu, Appl. Phys. Lett. 29, 707 (1976).
[16]M. Ackerman and F. Biaume, J. Mol. Spectrosc. 35, 73 (1970).
[17]L. Wolniewicz, J. Chem. Phys. 51, 5002 (1969).
[18]Ewald H. Fink, Daniel L. Akins, and C. Bradley Moore, J. Chem. Phys. 59, 900 (1972).
[19]R. J. Spindler, J. Quant. Spectrosc. Radiat. Transf. 9, 1041 (1969).
[20]W. L. Fite, R. T. Brackmann, D. G. Hummer, and R. F. Stebbings, Phys. Rev. 116, 363 (1959); 124, 2051 (1961).
[21]S. R. Ryan, S. J. Czuchlewski and M. V. McCusker, Phys. Rev. A 16, 1892 (1977).
[22]Joel I. Gersten, J. Chem. Phys. 51, 637 (1969).
[23]C. A. Slocomb, W. H. Miller, and H. F. Schaeffer III, J. Chem. Phys. 55, 926 (1971).
[24]Daniel J. Kligler, thesis, Stanford University, 1979 (unpublished).
[25]R. J. Cross, Jr., and R. G. Gordon, J. Chem. Phys. 45, 3571 (1966).
[26]J. O. Hirschfelder and W. J. Meath, Adv. Chem. Phys. 12, 3 (1967).
[27]A. R. Edmonds, *Angular Momentum in Quantum Mechanics* (Princeton University, Princeton, N. J., 1957).
[28]*Handbook of Mathematical Functions*, edited by Milton Abramowicz and Irene A. Stegun (National Bureau of Standards, Washington, D. C., 1964), p. 556.
[29]W. Kolos and L. Wolniewicz, J. Chem. Phys. 41, 3674 (1964).
[30]C. S. Lin, J. Chem. Phys. 60, 4660 (1974).
[31]A. C. Allison and A. Dalgarno, At. Data 1, 289 (1970).
[32]B. R. Marx, J. Simons, and L. Allen, J. Phys. B 11, 1273 (1978).
[33]Arthur Cohn, J. Chem. Phys. 57, 2456 (1972).
[34]*The Hydrogen Molecule Wavelength Tables of Gerhard Heinrich Dieke*, edited by H. M. Crosswhite (Wiley, New York, 1972).
[35]W. F. Heukels and J. Van de Ree, J. Chem. Phys. 57, 1393 (1972).
[36]M. Mitchner and C. H. Kruger, *Partially Ionized Gases* (Wiley, New York, 1973).
[37]R. M. Jonkman, G. J. Prangsma, and J. J. M. Beenakker, *Sixth Rarefied Gas Dynamics* (Academic, New York, 1969), p. 1413.
[38]Daniel L. Akins, Ewald H. Fink, and C. Bradley Moore, J. Chem. Phys. 52, 1604 (1970).